Feasibility Study for Reconstructing the Spatial-Temporal Structure of TIDs from High-Resolution Backscatter Ionograms[1]

L. J. Nickisch, Sergey Fridman, Mark Hausman, Geoffrey S. San Antonio*
NorthWest Research Associates, 301 Webster St., Monterey, CA 93940
* Naval Research Laboratory, Radar Division

Over-the-Horizon radar (OTHR) utilizes the reflective "skywave" property of the ionosphere for High Frequency radiowaves to illuminate targets at ranges extending to several thousand kilometers. However, the ionospheric "mirror" is not static, but exhibits geographic, diurnal, seasonal, and solar cycle variations. NorthWest Research Associates (NWRA) has developed an ionospheric data assimilation capability called Global Positioning Satellite Ionospheric Inversion (GPSII; pronounced "gypsy") that allows real-time modeling of the ionospheric structure for the purpose of accurate Coordinate Registration (CR; geolocating targets illuminated by HF skywave modes). However, the ionosphere is routinely subjected to wavelike perturbations known as Traveling Ionospheric Disturbances (TIDs), and the deflection of HF skywave signals by unmodeled TIDs remains a troubling source of CR errors (tens of kilometers). Traditional OTHR tools for ionospheric sounding (vertical and backscatter ionograms) do not resolve the fine spatial structure associated with TIDs. It was demonstrated recently that it is possible to collect backscatter ionograms using the full aperture of the OTHR, thus providing enhanced resolution in radar steer in comparison with conventional OTHR backscatter soundings that utilize only a fraction of the OTHR receiver array. Leading edges of such backscatter ionograms demonstrate prominent spatial features associated with TIDs. In this paper we investigate the feasibility of recovering TID perturbations of ionospheric electron density from high-resolution backscatter ionograms. We incorporated a model of naturally-occurring TIDs into a numerical ray tracing code that allows the generation of synthetic OTHR data. We augmented GPSII to be able to assimilate time series of full-aperture backscatter ionogram leading edge data. Results of the simulation show that GPSII inversion is able to reproduce the true TID structure reasonably well.

1. Introduction

Our team at NorthWest Research Associates (NWRA) is the developer of an OTHR CR capability called CREDO (Coordinate Registration Enhancement by Dynamic Optimization) [*Fridman*, 1998; *Fridman and Nickisch*, 2001; *Nickisch, et al*, 1998]. CREDO uses OTHR vertical and oblique backscatter soundings to model the ionosphere by applying Tikhonov's methodology [*Tikhonov and Arsenin*, 1977] for solving ill-posed problems (extended to multidimensional nonlinear inverse problems and optimized for fast numerical solution). The application of Tikhonov Regularization produces the smoothest ionosphere that is in agreement with the input data to within the data measurement error. More recently we developed the Tikhonov-based ionospheric data assimilation capability called GPSII [*Fridman, et al.*, 2006; 2009; 2012; *McNamara, et al.*, 2013]. GPSII is capable of ingesting data from GPS and low earth orbiting (LEO) satellite beacons, *in situ* electron density (e.g., DMSP or CHAMP satellites), the Jason altimeter, the DORIS system, and vertical incidence sounders to derive a three-dimensional ionosphere model that is both spatially and temporally smooth, but is yet in agreement with all the input data to within the data measurement error. In a previous effort we added the CREDO CR functionality to GPSII to make GPSII the basis of the way forward for the next generation of OTHR CR systems. We extended GPSII to incorporate the one-hop leading edge data from OTHR backscatter ionograms [*Fridman, et al.*, 2011; 2013].

For the Relocatable Over-the-Horizon Radar (ROTHR), these backscatter ionograms are referred to as Wide-Sweep Backscatter Ionograms (WSBIs). A synthesized example of a WSBI is shown on left hand side of Figure 1. This example was generated by NWRA's HiCIRF code, which applies numerical ray tracing in a climatological ionosphere model to generate realistic OTHR data [*Nickisch, et al.*, 2012]. In this figure,

[1] This research is based upon work supported in part by the Air Force Research Laboratory under contract FA9453-13-M-0190. The views and conclusions contained herein are those of the authors and should not be interpreted as necessarily representing the official policies or endorsements, either expressed or implied, of AFRL or the U.S. Government. The U.S. Government is authorized to reproduce and distribute reprints for Governmental purposes notwithstanding any copyright annotation thereon.

"Slant Range" refers to time delay times the speed of light (divided by two) and represents the radar sounding delay from ground (or ocean) backscatter points as a function of radar operating frequency. Features related to one-, two-, and three-hop skywave propagation modes are apparent (WSBI lobes) as well as finer structure associated with the details of HF propagation modes in the layered ionosphere. The leading edge of the one-hop WSBI lobe (the shortest slant range return at each frequency) is a characteristic, easily identifiable feature that is used by CREDO and GPSII to model the down-range ionosphere away from the radar. Note that the leading edge in this example is very sharply defined, since in this synthetic example the WSBI can be generated with infinitesimal beam resolution.

ROTHR, however, uses only a fraction of the linear receive array (the end 28 elements of the 372 element array) to measure WSBIs; the azimuthal width of a ROTHR WSBI sector is about 10 degrees. Because of the large angular width of the sounder receive beam, the characteristic "leading edge" feature of the WSBIs is a blurred image of the minimum-delay propagation modes over that width. An example of a real measured WSBI is shown on the right in Figure 1. Notice that the one-hop leading edge is less well defined than in the synthetic example on the left. Also note that there is some structure evident on the leading edge of the real measurement that appears as a slight "wander" of the leading edge about its roughly linear trend upward with frequency. We will show that this structure is likely related to TIDs.

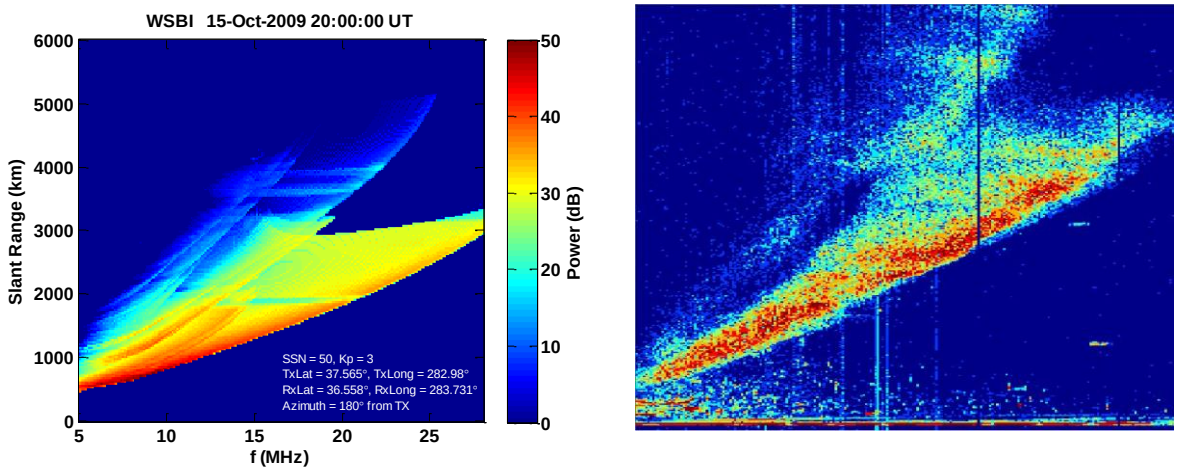

Figure 1. Left: Synthetic Wide-Sweep Backscatter Ionogram generated by HiCIRF. Right: Example of a real measured WSBI.

We have implemented the TID model of Hooke [1968] into a variant of the well-known Jones-Stephenson ray tracing code [*Jones and Stephenson*, 1975]. We generated synthetic data sets corresponding to OTHR backscatter soundings with an azimuthal resolution substantially higher than that routinely measured by the ROTHR. By using a larger portion of the receive aperture, finer resolution WSBI leading edges could conceptually be obtained (and have been obtained experimentally, as we will show in the next section), and we will show that structure related to any TIDs that are present can be exposed. In our simulations, we used an angular beam resolution of 2 degrees, which roughly corresponds to using 80% of the ROTHR receive aperture at the lowest frequencies, and we found this resolution to be adequate for resolving medium-scale TIDs of 300 km wavelength. We then incorporated the ability to assimilate the high-angular-resolution WSBI leading edge data into GPSII, and we demonstrated that the corresponding ionosphere model solution well-matches the input TID structure used to generate the synthetic WSBI data.

This paper is organized as follows. In Section 2 we describe the motivation for assimilating high-angular-resolution backscatter sounding leading edge data in GPSII based on real ROTHR measurements. In Section 3 we describe our incorporation of the Hooke TID model as a perturbation model in our numerical ray tracing code. In Section 4 we describe the extension of GPSII for assimilating the high-angular-resolution backscatter sounding leading edge data and the encouraging results obtained in reproducing the TIDs used to generate synthesized WSBI leading data. Concluding remarks are given in Section 5.

2. Motivation for Resolving TID Structure in OTHR Backscatter Ionograms

Normally the ROTHR system collects Wide-Sweep Backscatter Ionograms (WSBIs) using a sub-array of the radar (the end 28 elements of the 372-element receiver array). This results in WSBIs with

approximately a 10 degree azimuthal beam, meaning that the WSBI signature of interest, the leading edge, represents the minimum delay return at each frequency over that 10 degree sector as weighted by the beam gain. Sometimes traveling ionospheric disturbance (TID) signatures are visible in these WSBI leading edges as distortions in delay as a function of frequency, but the poor resolution in the azimuthal dimension makes it difficult to resolve the signatures for modeling purposes. However, using the ROTHR-Virginia radar in a special mode of operation, Dr. San Antonio of the US Naval Research Laboratory was able to collect WSBI data using the full radar aperture for a limited frequency band. With the full receive aperture, the angular resolution of the ROTHR is 0.5 degrees or better at the higher frequencies, degrading to about 1.5 at the lowest operational frequencies. This angular resolution is adequate to resolve TIDs. An example is shown in Figure 2. The plot on the left of Figure 2 was produced by Dr. San Antonio by performing a full-aperture backscatter sounding with ROTHR and extracting the leading edges of the sounding over the frequency band from 15 to 27 MHz. There are some edge artifacts that can be ignored, but TID structure is definitely apparent, especially in the circled region. That these undulations are due to TIDs is corroborated by NWRA analysis. On the right of Figure 2 we show the result of a numerical ray trace simulation using a simple plane wave perturbation of the ionosphere for a region approximately the same as the circled region on the left pane. While we did only minor tuning of the plane wave amplitude, wavelength, and direction parameters (so one shouldn't expect exact reproduction), it is clear that our synthetic TIDs produce a very similar undulating structure as the full-aperture backscatter sounding.

The fact that TID information is encoded in the backscatter sounding leading edges and is readily observable in high-angular-resolution WSBIs provides hope that an ionospheric inversion algorithm like GPSII might be able to model the underlying TID structure if the leading edge data is assimilated. This would be an excellent way of mitigating TID effects on CR because 1) backscatter soundings are routinely collected by OTHRs (albeit not usually with high angular resolution), 2) the backscatter soundings cover exactly the operational field of view of the radar, and 3) modern digital technology will allow a next generation system to perform backscatter soundings using the full receive aperture without impacting the surveillance mission of the radar. In the following sections we will explore, through simulation, the degree to which the goal of assimilating high-angular-resolution to model TIDs affecting OTHR CR can be accomplished.

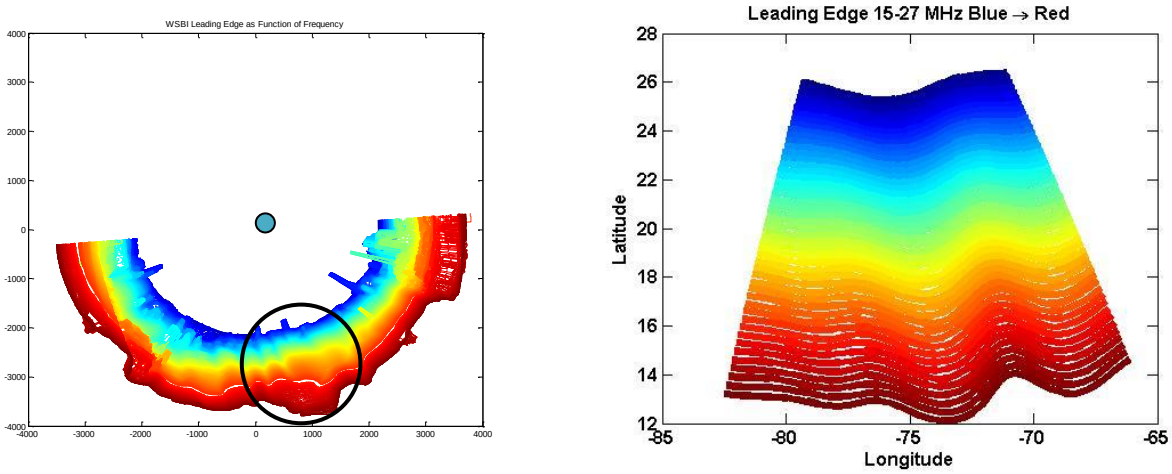

Figure 2. Left: High-resolution WSBI leading edges from measurements. Right: Simulation roughly corresponding to the circled region on the left pane.

3. Simulation of OTH Backscatter Sounding Data in the Presence of TIDs

3.1 Dynamic model for traveling ionospheric disturbances

For this study, we have implemented a model for natural TIDs that is parameterized by the TID wavelength so we can look at whatever scales of structure we choose. The model is that of *Hooke* [1968; *see also Cervera and Harris*, 2014]. As implemented in our code, the TID perturbation to a background electron density distribution $N_{e0}(\mathbf{x})$ is given by

$$N_e'(\mathbf{x}) = N_{e0}(\mathbf{x}) U_b(z_0) \sin(I) \exp(k_{zi}(z - z_0)) \omega^{-1} \sqrt{\left(\frac{\partial \ln N_{e0}}{\partial z} + k_{zi}\right)^2 + \left(\frac{k_{br}}{\sin I}\right)^2}$$
$$\exp\left\{ i \left[\omega t - \mathbf{k} \cdot \mathbf{x} - \tan^{-1}\left(k_{br} \Big/ \sin I \left(\frac{\partial \ln N_{e0}}{\partial z} + k_{zi} \right) \right) \right] \right\}. \quad \textbf{(1)}$$

Here $U_b(z_0)$ is the magnitude of neutral gas velocity at a reference height z_0, which we take to be 250 km. I is the geomagnetic inclination, $k_{zi}=1/(2H)$ where H is the atmospheric scale height (at z_0), and k_{br} is the real part of the component of the TID wave vector **k** along the geomagnetic field,

$$k_{br} = \mathrm{Re}\left(\frac{\mathbf{k} \cdot \mathbf{B}_E}{|\mathbf{B}_E|} \right). \quad \textbf{(2)}$$

The scale height H is calculated using the Boltzmann constant k_B, temperature T, the mean molecular mass of the atmospheric constituents μ_{ave}, and the atomic mass unit m_u as,

$$H = \frac{k_B T}{\mu_{ave} m_u g}. \quad \textbf{(3)}$$

As in *Cervera and Harris* [2014], we have implemented the NRLSISE-00 model of the neutral atmosphere [*Picone et al.*, 2002] to specify T and μ_{ave}.

3.2 Simulation of backscatter sounding data in the presence of TIDs

The Hooke TID model is implemented in our ray tracing code (a modified version of the well-known *Jones-Stephenson* ray tracing code [*Jones and Stephenson*, 1975]) as an electron density perturbation model. This way we can use any underlying background electron density model available to our code, including the International Reference Ionosphere (IRI) or our own GPSII-derived ionosphere models. There was a bit of a trick in implementing this model as a perturbation model to get the spatial derivatives right; ray tracing requires first spatial derivatives of electron density and our power calculations require second spatial derivatives. We resorted to computing finite-difference derivatives, which is normally not a problem, but since the model already depends on a derivative of the background electron density, computing the perturbed values at discretely separated points required calling the main electron density routine recursively. By setting a flag so that the perturbation routine would not be called when recursively calling the higher-level routine, we were successful in the recursive implementation (and the compiler allowed it!). An example of the Hooke TID model is shown in Figure 3.

We would like to test the ability of our ionospheric data assimilation code GPSII to resolve TID structure from Wide-Sweep Backscatter Ionograms (WSBIs) that are obtained using the full OTHR receive aperture. Currently the ROTHR system uses only a sub-array of the full receive aperture to collect WSBIs, resulting in a relatively low azimuthal resolution of the WSBIs at about 10º that blurs the leading edge of the WSBI lobes. For the data shown in Section 2, a special mode of operation was used to collect WSBIs using the full receive aperture, resulting in WSBI leading edges resolved to about a half degree. In these measurements, structure appeared that we showed using a simple perturbations model, were consistent with TIDs. To simulate this with the new Hooke TID model in our ray tracing code, we wrote a Matlab script for generating lists of azimuths for rays at different elevations corresponding to equally-spaced fixed steers of the radar, that is, to account for "coning" of the linear receive array. Coning refers to the fact that when a linear array is steered to a given azimuthal direction at zero elevation, its elements are phased respectively so that higher elevations come in at azimuths that form a cone around the axis of the linear array. Our Matlab script

computes these coning angles for ray fans in elevation at a set of steers (spanning ±45º from boresight in the following example).

Figure 4 illustrates a snapshot of synthetic WSBI leading edge data produced by the above outlined algorithm. Lines of different color correspond to different sounding frequencies. Frequencies are spanning 10-24 MHz (every 2 MHz; dark blue color corresponds to 10 MHz, and dark brown color corresponds to 24 MHz). The plot is labeled in conventional geographic coordinates. However, the apparent ground range of each point of the plot from the radar location (37.1N, -76.6E) is equal to the value of the leading edge slant range, while the azimuth of each point (as viewed from the radar location) is equal to the radar steer angle measured from North. The ray tracing results are written into an output file that we can access to find the range minima and write our standard files that contain leading edge information for GPSII processing. Such data sets were generated for a 60 minute time interval starting at 1900UT, 15 January, 2014 with the step of 2 minutes.

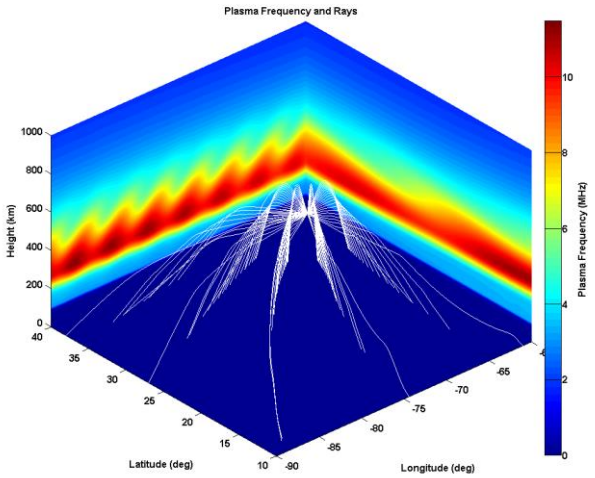

Figure 3. Slices of a Hooke TID-perturbed ionosphere and traced elevation fans of rays at 15 MHz.

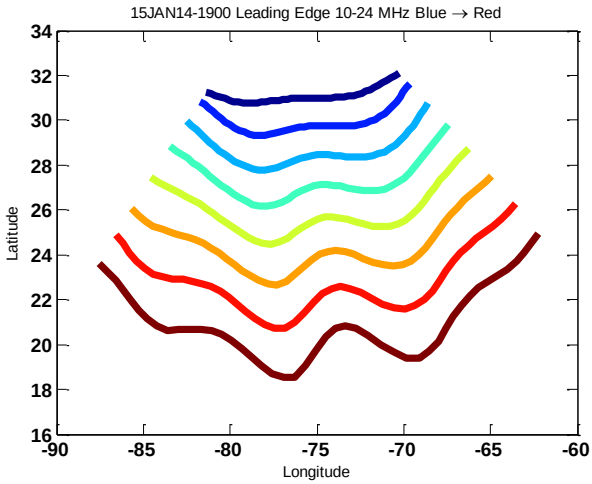

Figure 4. Synthetic WSBI leading edges at a set of frequencies spanning 10-24 MHz (every 2 MHz) and ±45º steer for an example Hooke TID in an IRI background ionosphere model.

Note the wiggles in the leading edge points shown in **Figure 4**. We show in the next section that our GPSII code is able to assimilate this information and produce a reasonable representation of the simulated ionosphere from which these simulated data are derived.

4. GPSII Assimilation of High-Angular-Resolution Backscatter Sounding Data

4.1 Modification of GPSII evolution equation

Our long-term goal is to develop a new version of GPSII that, to a certain degree, would exploit the physics of TID propagation and evolution. In order to accomplish this we must to modify the evolution equation that projects the solution to the next time step. Originally the algorithm employed the equation [*Fridman et al.*, 2006]

$$U_n = \gamma U_{n-1} + \nu_n \qquad \textbf{(4)}$$

where U_{n-1} is the modification vector at the time step *n*-1, γ, $0 < \gamma < 1$ is the attenuation coefficient, and ν_n is the correction vector. This equation represents a first order linear process. Such a process is not suitable for simulating the oscillating behavior that is characteristic for TID phenomena. Only higher-order linear processes can in principle exhibit oscillating solutions. With this in mind we are replacing (4) with a more flexible second-order process:

$$U_n = \gamma_1 U_{n-1} + \gamma_2 U_{n-2} + \nu_n . \qquad \textbf{(5)}$$

The coefficients γ_1 and γ_2 can be conveniently related to the attenuation time scale τ_s and the intrinsic oscillation period *T*. In order to obtain this relationship we require that the decaying oscillating functions $u_n = \exp(-t_n/\tau_s + it_n 2\pi/T)$ and $\nu_n = \exp(-t_n/\tau_s - it_n 2\pi/T)$ satisfy the uniform version of equation (5). Here temporal nodes of the solution t_n are assumed to be uniformly spaced. With the help of the Vieta's formulas we find:

$$\begin{aligned} \gamma_1 &= 2e^{-\frac{\Delta t}{\tau}} \cos\frac{2\pi\Delta t}{T} \\ \gamma_2 &= -e^{-2\frac{\Delta t}{\tau_s}} \end{aligned} . \qquad \textbf{(6)}$$

where $\Delta t = t_n - t_{n-1}$. The second order system (5) can also support aperiodic (non-oscillating) eigensolutions. Such aperiodic systems can be specified by two temporal scales - the fast attenuation time τ_f and the slow attenuation time $\tau_s \geq \tau_f$. Then $\exp(-t_n/\tau_f)$ and $\exp(-t_n/\tau_s)$ must be eigensolutions for the uniform version of the equation (5) yielding the following values for coefficients:

$$\begin{aligned} \gamma_1 &= e^{-\frac{\Delta t}{\tau_s}} + e^{-\frac{\Delta t}{\tau_f}} \\ \gamma_2 &= -e^{-\frac{\Delta t}{\tau_s} - \frac{\Delta t}{\tau_f}} \end{aligned} . \qquad \textbf{(7)}$$

We observe that as $\tau_f \to 0$, $\gamma_2 \to 0$, meaning that the evolution equation reduces to the first order system (4). In the case of $\tau_s, \tau_f \to \infty$ we get $\gamma_1 = 2$, $\gamma_2 = -1$, meaning that the evolution equation (5) provides straightforward linear extrapolation in time. In general equation (5) with coefficients (7) provides linear extrapolation with damping.

Parameters τ_s, τ_f or τ_s, T should be set at the start of a GPSII run based on expected variability of the ionosphere and the temporal step of the inversion. So far we have only experimented with aperiodic evolution equations. This way we are confident that any oscillating behavior of the solution is driven by data, rather than by parameters of the model. The TID-related GPSII solution presented in Section 4.3 below employs Δt =2 min, τ_s =50 min, and τ_f =10 min.

4.2 Work on speeding up GPSII processing of HF data

In future usage we intend to operate GPSII with a considerable load of HF data such as beacon observations, WSBI leading edges, or the ionospheric Doppler observed in ground clutter. In these conditions, the HF numerical ray-tracing tasks tend to be the slowest component of the computation process. We are revising elements of the GPSII code with the intention of speeding up the ray tracing.

Ray tracing requires numerous calculations of the plasma density. The plasma density information is stored in a three-dimensional table, so that each calculation of the density invokes a three-dimensional interpolation. The ray tracing equations are very sensitive to the smoothness of the medium, so we are employing a tri-cubic local spline interpolation that provides continuity of first derivatives through the whole region. We have reviewed our interpolation algorithm for the possibility of benefitting from the research published by Lekien and Marsden [2005]. We concluded that our 3-D interpolation may be accelerated by employing the formalism of the one-dimensional interpolation method known as the Catmull–Rom spline [*Catmull and Rom*, 1974].

In the case of a function of one variable, the Catmull–Rom spline interpolation can be expressed as

$$F(x) = \sum_{\alpha=-1}^{2} f_{i+\alpha} v_\alpha \left(\frac{x - x_i}{x_{i+1} - x_i} \right), \; x_i \le x < x_{i+1} \tag{8}$$

where f_i represents the table of the function being interpolated and, in the case of uniformly spaced nodes x_i, the interpolation coefficients are

$$v_{[-1:2]}(t) = \frac{1}{2} \begin{bmatrix} -t^3 + 2t^2 - t \\ 3t^3 - 5t^2 + 2 \\ -3t^3 + 4t^2 + t \\ t^3 - t^2 \end{bmatrix} \tag{9}$$

In the general case of a non-uniformly spaced grid we derived the following expressions for the coefficients:

$$v_{[-1:2]}(t) = \begin{bmatrix} \frac{1}{d_-(1+d_+)}(-t^3 + 2t^2 - t) \\ (2 - \frac{d_+}{1+d_+} + \frac{1-d_-}{d_-})t^3 - (3 + 2\frac{1-d_-}{d_-} - \frac{d_+}{1+d_+})t^2 + \frac{1-d_-}{d_-}t + 1 \\ (-2 + \frac{d_-}{1+d_-} + \frac{d_+ - 1}{d_+})t^3 + (3 - 2\frac{d_-}{1+d_-} - \frac{d_+ - 1}{d_+})t^2 + \frac{d_-}{1+d_-}t \\ \frac{1}{d_+(1+d_+)}(t^3 - t^2) \end{bmatrix} \tag{10}$$

where $d_- = \frac{x_i - x_{i-1}}{x_{i+1} - x_i}$, and $d_+ = \frac{x_{i+2} - x_{i+1}}{x_{i+1} - x_i}$. Note that on the border between two adjacent intervals [i-1,i] and [i,i+1] the value of the first derivative of the interpolated function is $\frac{f_i - f_{i-1}}{x_i - x_{i-1}} \frac{x_{i+1} - x_i}{x_{i+1} - x_{i-1}} + \frac{f_{i+1} - f_i}{x_{i+1} - x_i} \frac{x_i - x_{i-1}}{x_{i+1} - x_{i-1}}$. This estimate is known to be accurate to the second order.

We are interested in interpolating a function of three variables that is specified by its values $f_{ijk} = F(x_i, y_j, z_k)$ over a rectangular three-dimensional grid. The following is the three-dimensional generalization of the Catmull–Rom spline:

$$F(x,y,z) = \sum_{\gamma=-1}^{2} \sum_{\beta=-1}^{2} \sum_{\alpha=-1}^{2} f_{i+\alpha, j+\beta, k+\gamma} v_\alpha^x \left(\frac{x - x_i}{x_{i+1} - x_i} \right) v_\beta^y \left(\frac{y - y_j}{y_{j+1} - y_j} \right) v_\gamma^z \left(\frac{z - z_k}{z_{k+1} - z_k} \right) \tag{11}$$
$$x_i \le x < x_{i+1}, y_k \le y < y_{k+1}, z_k \le z < z_{k+1}$$

Note that for each evaluation of the function F, the vectors $v^x_{[-1:2]}$, $v^y_{[-1:2]}$, and $v^z_{[-1:2]}$ are calculated in accordance with (10) or (9). These spline coefficients need to be evaluated only once per interpolation, which compares favorably with the older version of our interpolation algorithm that required 21 evaluations of the one-dimensional cubic spline per interpolation. There is a potential for very efficient computer evaluation of the expression (11) using vectorized processing.

The algorithm described above is now implemented for plasma density calculations in the GPSII ray tracing codes. We are observing approximately 30% reduction in computation time while the resulting solutions remain virtually identical to solutions obtained with the old algorithm.

We used an Intel Fortran Compiler that performs automatic vectorization of calculations. Detailed analysis of the compilation log revealed that the compiler failed to detect the opportunity for vectorization in

the code representing expression (11). In the near future we plan to introduce appropriate vectorization control directives into the code. Thus, further reduction in computation time is expected.

4.3 GPSII reconstruction of the TID-affected ionosphere

Our main goal is to assess whether high-resolution OTHR backscatter sounding data may be useful for determining transient medium-scale perturbations of electron density such as TIDs. For this purpose we generated simulated high-resolution WSBI leading edge data for ROTHR Virginia by conducting ray-tracing through the TID-perturbed ionosphere as described in Section 3. These simulated measurements were then fed into GPSII inversion which produced the three-dimensional distribution of electron density as a function of time.

The simulated leading edge measurements covered the time interval of one hour sampled every 2 minutes, starting at 1900UT of January 15, 2014. Radar steer angles of the WSBI data extended from -45 to +45 degrees with a step of 2 degrees. The leading edge samples were generated at 8 frequencies from 10 MHz to 24 MHz with the step of 2 MHz for each of the 46 values of the steer angle. That is, GPSII was processing 368 leading edge samples at each time step of this numerical experiment. In addition to that, GPSII was assimilating the time series of vertical profiles of electron density over the location WSBI sounder. (For this simulation, the backscatter sounder was treated as a monostatic sounder positioned at the midpoint between the ROTHR-Virginia transmitter and receiver locations.)

A sequence of the synthesized WSBI leading edge data is shown in Figure 5. These plots are separated in time by 4 minutes (and represent the same times for the GPSII solution snapshots shown later in Figure 6). Note that the ripples of the TID-generated structure progress to the right over time, and after twenty minutes the structure in the lower right (last) frame is similar to the structure in the upper left (first) frame, indicating a 20 minute period for this TID. Slight differences between the first and last frame are due to the evolution of the underlying IRI climatological model over this 20 minute period.

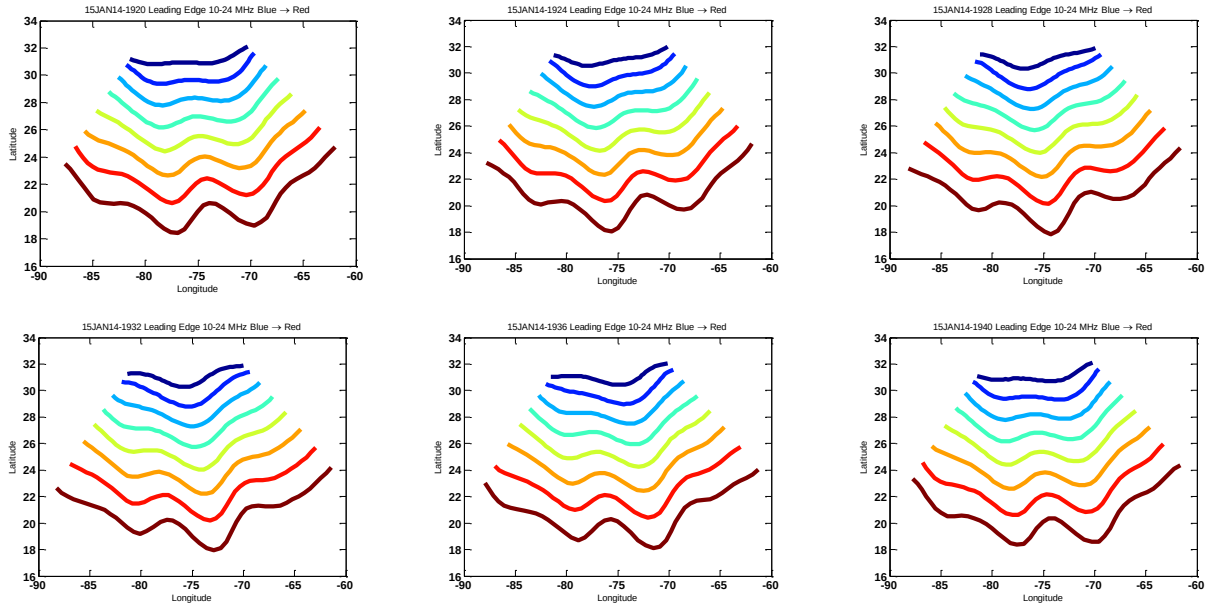

Figure 5. Sequence of WSBI leading edge plots similar to Figure 4, separated in time by 4 minutes.

In the results shown below we assumed that the accuracy of leading edge measurements is characterized by a standard deviation of 25 km. During the solution we observed good convergence of the algorithm. At every time step GPSII converged after just one non-linear iteration. This means that GPSII's linear operator, that approximates the relation of the leading edge data to the distribution of electron density in the ionosphere, provides extremely good accuracy for TIDs of moderate magnitude. We also noticed that the new evolution equation (5) appears to be beneficial; we observed that at the beginning of each time step the mean-square misfit between the data and the GPSII-modeled data is at least factor of 2 smaller when equation (5) is employed instead of equation (4).

A horizontal slice through two GPSII solutions at the altitude of 250 km is shown in **Figure 6**. This altitude is chosen as a representative value for the altitude of reflection of rays forming WSBI leading edge. The separation of the snapshots in time is 4 minutes. One can observe a wave-like disturbance within the radar coverage sector (black dashed line) propagating approximately eastward. The temporal period of the disturbance is approximately 20 minutes and the horizontal wavelength is about 430 km. These values are consistent with truth: 20 minutes and 300/sin(45)=423 km, respectively (the Hooke TID model used a 300 km wavelength with a -45º inclination of propagation). The true wave is propagating eastward at an azimuth of 80º east of north.

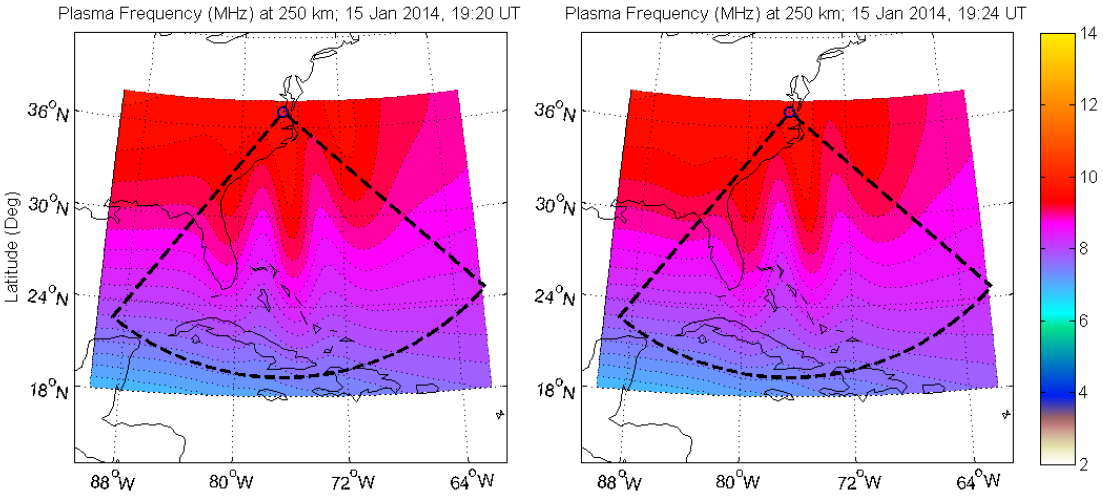

Figure 6. GPSII solution assimilating high resolution WSBI leading edge data.

A different visualization of the eastward propagating wave in GPSII solution is shown in Figure 7. Here is shown vertical slices through the solution at the constant latitude of 28N (about 1000 km from the radar) with a time step of 6 minutes. Figure 7 shows comparison of the true distribution of electron density (as it was used for generating the leading edge data) with the GPSII solution. The accuracy of the reconstruction appears to be quite good within the region of support of the WSBI coverage; the TID perturbation reconstructed by GPSII is restricted to the radar coverage area in this simulation because there were no sources of ionospheric information outside of the area. We note, however, that there is a slight lag in the GPSII solution progression over time of the TID structure relative to the truth. This is because we do not have knowledge of the actual TID wave propagation physics built into the GPSII solution, something we hope to rectify in future work. We see two directions of future work to improve this situation.

One direction is to invoke other kinds of ionospheric measurements that would represent the ionosphere outside of the radar coverage area. TEC data from ground-based GPS receivers are most-readily available. The capability to ingest this kind of data is already present in the algorithm. In future we plan to produce simulated GPS TEC data (in addition to the leading edge data) in order to evaluate whether this type of measurements can help to extend reconstructed TID perturbations outside of the radar coverage area.

Another direction is to modify GPSII evolution equation to incorporate propagating disturbances. Indeed, neither of our versions of evolution equations (4), or (5) accounts for TID propagation effects. We plan to generalize the evolution equation so that TID perturbations would be propagated beyond the radar coverage area consistently with the physics of this phenomenon.

The speed of the algorithm when operated with high-resolution HF data is currently lagging behind the desired real-time performance. We plan to resolve this issue. General revision of the code needs to be done to implement parallel computations as well as vector processing in ray-tracing related tasks. Also we plan to look into algorithm improvements which are specific for high-resolution, high-sampling-rate data. Namely we want to study how we can exploit the above-mentioned observation that the system behaves close to a linear system when we are dealing with fairly high sampling rates (~1 sample/minute) which are necessary for tracking TID perturbations.

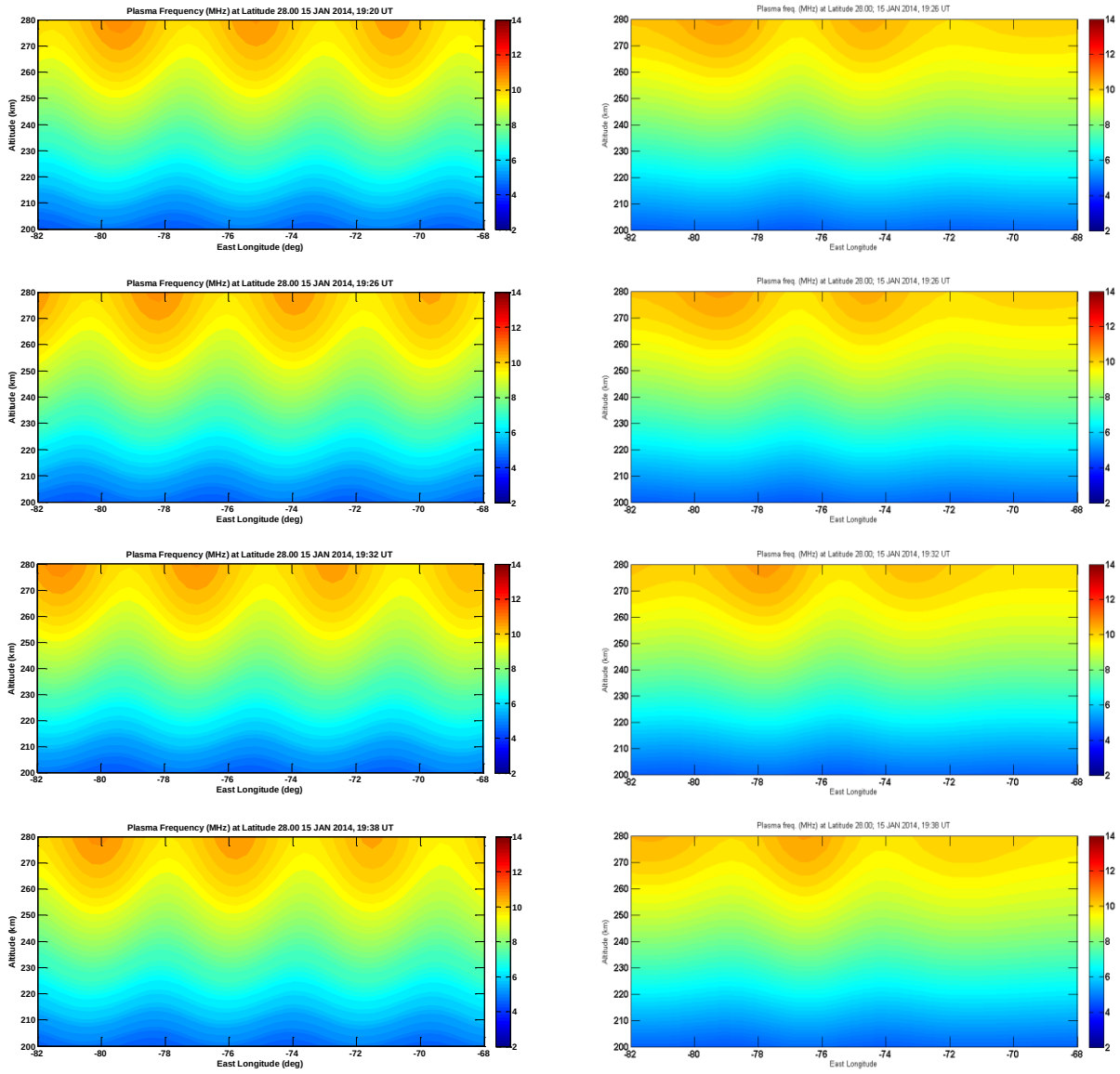

Figure 7. Longitude-altitude cross-section of (left) Hooke TID model and (right) GPSII solution every 6 minutes.

5. Conclusion

We have incorporated the flexible TID model of Hooke [1968] in a numerical ray tracing code to generate synthetic OTHR sounding data. Specifically we generated Wide-Sweep Backscatter Ionograms (WSBIs) that correspond to what could be collected with an OTHR using its full receive aperture, or at least a significantly larger portion of its aperture than is conventionally used today, resulting in finer angular resolution and thereby a finer definition of the WSBI leading edges as a function of delay, frequency, and angle. We demonstrated that this exposes signatures in the WSBI leading edges of Traveling Ionospheric Disturbances (TIDs). We then demonstrated, using an extended version of our ionospheric data assimilation code, GPSII, that these signatures could be inverted to successfully reproduce the TID structures in the ionosphere within the region of support of the sounding data.

The Hooke TID model was implemented in our ray tracing code as an electron density perturbation model. This means it can be employed using any background ionosphere model one chooses. For the purpose of the study reported here, we used the International Reference Ionosphere (IRI) climatological model, but it is worth pointing out that we can also use the model ionospheres that are output by GPSII, or other model ionosphere models that are available to the ray tracing code.

The synthetic WSBI and vertical profile data we generated corresponded to a dynamic disturbed ionosphere; we generated one hour's worth of sounding data, every two minutes. The data assimilation code, GPSII, is a dynamic code that accepts time evolving data and generates a time evolving ionosphere model. We chose a two-minute sampling rate for the WSBI data since this seemed adequate for resolving the TID structures temporally and is an achievable rate for the next generation of radar backscatter sounding collection and processing.

We improved the speed and predictive capabilities of the GPSII inversion algorithm to handle large arrays of HF data, such as the high-resolution leading edge data employed in this study. The improved GPSII was used to invert the synthetic leading edge data. Our comparison of the GPSII output model with the truth model as very favorable. We demonstrated that GPSII ionospheric model is quite sensitive to the TID-affected backscatter leading edge data. The TID perturbation of electron density in the bottom-side ionosphere is reconstructed by GPSII with good accuracy.

In our ongoing work we plan to develop the GPSII algorithm further so that physics-based or observations-based TID propagation equations are incorporated within the algorithm. The current GPSII algorithm is flexible enough to model the TID structures when data of sufficient resolution is available (like the full-aperture WSBI leading edge data), but the algorithm is ignorant of the actual propagation of the TIDs. We believe that it will be possible to incorporate enough information about the TIDs that their propagation can be predicted to a significant level. When this is accomplished, GPSII will be able to intelligently evolve the TIDs ahead in time. This will make the starting solution for the next GPSII time step closer to the actual one, decreasing GPSII's convergence time and possibly allowing the use of sparser data both temporally and spatially.

We also intend to revise the GPSII algorithm to improve the speed of its ray tracing computations, including specific improvements for dealing with high-resolution, high-sampling-rate HF data.

We plan to further evaluate the TID diagnostic capability of GPSII driven by GPS TEC and other HF data, especially HF Doppler data. In the past we explored the use of the Doppler shifts of OTHR surface backscatter clutter to mitigate TID CR estimates using a mutual regression approach that required a training data set in lieu of performing actual ionospheric inversion [Nickisch, et al., 2007]. However, since that time we have incorporated into GPSII the linearized ray path response operator, which describes how a ray path deviates when a sample of the electron density along its path is perturbed. With this it will now be possible to actually invert the surface-clutter Doppler-shift characteristics to obtain the corresponding ionospheric perturbations that cause the Doppler shifts. This, when coupled with the full-aperture WSBI inversion technique will, we believe, form the basis of next-generation high-fidelity CR.

Finally, we plan to test these developments using real OTHR system data and diagnostic measurements. We plan to measure full aperture WSBIs using an existing OTHR. We also hope to have a separate HF Doppler sounder near the midpath of a link from the OTHR to a fixed transponder. The Doppler sounder consists of a central receiver inside a triangle of HF transmitters separated by about 100 km. Doppler shifts in the transmitted signals are correlated over space and time to infer the number, directions, magnitudes, wavelengths, and speeds of TIDs affecting the reflection points of the three links. We will be able to determine how well the GPSII-inverted TIDs correlate with those elucidated by the midpath Doppler sounder, and separately the Doppler sounder data can be assimilated by GPSII to explore the potential utility of Doppler sounder data to improve OTHR CR.

References

Cervera, M. A., and T. J. Harris, "Modeling ionospheric disturbance features in quasi-vertically incident ionograms using 3-D magnetoionic ray tracing and atmospheric gravity waves," J. Geophys. Res. Space Physics, 119, doi:10.1002/2013JA019247, 2014

Fridman, Sergey V., "Reconstruction of three-dimensional ionosphere from backscatter and vertical ionograms measured by over-the-horizon radar," Radio Science, V. 33, No 4, pp. 1159-1171, 1998.

Fridman, Sergey V. and L. J. Nickisch, "Generalization of ionospheric tomography on diverse data sources: Reconstruction of the three-dimensional ionosphere from simultaneous vertical ionograms, backscatter ionograms, and total electron content data," Radio Science, Vol. 36, Number 5, September-October 2001.

Fridman, Sergey V., L. J. Nickisch, Mark Aiello, and Mark A. Hausman "Real time reconstruction of the three-dimensional ionosphere using data from a network of GPS receivers" Radio Science, 41, RS5S12, doi:10.1029/2005RS003341, 2006.

Fridman, Sergey V., L. J. Nickisch, and Mark Hausman, "Personal-computer-based system for real-time reconstruction of the three-dimensional ionosphere using data from diverse sources," Radio Science, 44, RS3008, doi:10.1029/2008RS004040, 2009.

Fridman, Sergey V., L. J. Nickisch, and Mark Hausman, "High Frequency Over-the-Horizon Radar Metric Accuracy – SBIR Phase I Final Report," Final Technical Report for AFRL contract FA9453-10-M-0104 (NWRA-SEA-10-R419), 2011.

Fridman, S. V., L. J. Nickisch, and M. Hausman, Inversion of backscatter ionograms and TEC data for over-the-horizon radar, Radio Sci., 47, RS0L10, doi:10.1029/2011RS004932, 2012.

Fridman, Sergey V., L. J. Nickisch, Mark Hausman, Greg Bullock, "High Frequency Over-the-Horizon Radar Metric Accuracy – SBIR Phase II Final Report," Final Technical Report for AFRL contract FA9453-11-C-0157 (NWRA-13-RM514), 2013.

Hooke, W. H., "Ionospheric irregularities produced by internal atmospheric gravity waves," Geophysical Monograph Series, *The Upper Atmosphere in Motion*, Vol. 18, pp. 780-808, 1968.

Jones, R. Michael and Judith J. Stephenson, A Versitile Three-Dimensional Ray Tracing Computer Program for Radio Waves in the Ionosphere, U.S. Department of Commerce OT Report 75-76

Lekien, F., and J. Marsden, Tricubic Interpolation in Three Dimensions, *International Journal of numerical Methods and Engineering*; **63**: 455–471, 2005.

McNamara, L. F., M. J. Angling, S. Elvidge, S. V. Fridman, M. A. Hausman, L. J. Nickisch, and L.-A. McKinnell, Assimilation procedures for updating ionospheric profiles below the F2 peak, Radio Sci., 48, doi:10.1002/rds.20020. 2013.

Nickisch, L. J., S. V. Fridman, and M. A. Hausman, Automated Propagation Management and Assessment for Over-the-Horizon Radar -- Final Technical Report, *AFRL Final Technical Report, MRC/MRY-R-070,* Air Force Research Laboratory, Hanscom AFB, MA, 1998.

Nickisch, L. J., M. A. Hausman , and S. V. Fridman, "Traveling Ionospheric Disturbance Mitigation for OTH Radar," Proceedings IEEE Radar 2007 Conference, 2007

Nickisch, L. J., Gavin St. John, S. V. Fridman, M. A. Hausman and C. J. Coleman , "HiCIRF: A High-Fidelity HF Channel Simulation," Radio Science, V.47, RS0L11, doi:10.1029/2011RS004928, 2012

Picone, J. M., A. E. Hedin, D. P. Drob, and A. C. Aikin, "NRLMSISE-00 empirical model of the atmosphere: Statistical comparisons and scientific issues," J. Geophys. Res. Space Physics, 107, 1468, doi:10.1029/2002JA009430, 2002

Tikhonov, A. N., and V. Y. Arsenin, Solution of Ill-Posed Problems, Halsted, New York, 1977.